

Differences in regional wash-in and wash-out time constants for xenon-CT ventilation studies

Deokiee Chon^a, Brett A. Simon^b, Kenneth C. Beck^a, Hidenori Shikata^a,
Osama I. Saba^a, Chulho Won^a, Eric A. Hoffman^{a,*}

^a Departments of Radiology and Biomedical Engineering, University of Iowa College of Medicine,
200 Hawkins Drive, Iowa City, IA 52242, USA

^b Department of Anesthesiology and Critical Care Medicine, The Johns Hopkins University, Baltimore, MD, USA

Accepted 7 June 2005

Abstract

Xenon-enhanced computed tomography (Xe-CT) has been used to measure regional ventilation by determining the wash-in (WI) and wash-out (WO) rates of stable Xe. We tested the common assumption that WI and WO rates are equal by measuring WO–WI in different anatomic lung regions of six anesthetized, supine sheep scanned using multi-detector-row computed tomography (MDCT). We further investigated the effect of tidal volume, image gating (end-expiratory EE versus end-inspiratory EI), local perfusion, and inspired Xe concentration on this phenomenon. Results: WO time constant was greater than WI in all lung regions, with the greatest differences observed in dependent base regions. WO–WI time constant difference was greater during EE imaging, smaller tidal volumes, and with higher Xe concentrations. Regional perfusion did not correlate with WI–WO. We conclude that Xe-WI rate can be significantly different from the WO rate, and the data suggest that this effect may be due to a combination of anatomic and fluid mechanical factors such as Rayleigh–Taylor instabilities set up at interfaces between two gases of different densities.

© 2005 Elsevier B.V. All rights reserved.

Keywords: Xenon; Inert gas dilution; Regional lung ventilation measurements; Computed tomography; Pulmonary imaging; Airway conductance; Multi-detector row CT

1. Introduction

Since Knipping and co-workers introduced the use of radioactive xenon (Xe) gas to understand regional

pulmonary function in 1955 (Knipping et al., 1955), this gas has been used in various forms as a contrast material in conjunction with different imaging modalities. Small volumes of radioactive Xe¹³³ was used in the early studies with scintillation cameras (Ball et al., 1962; Bunow et al., 1979; van der Mark et al., 1980, 1984) and later single photon emission tomography (SPECT) (Suga et al., 1996; Almquist et al., 1999),

* Corresponding author. Tel.: +1 319 356 1381;
fax: +1 319 356 1503.

E-mail address: eric-hoffman@uiowa.edu (E.A. Hoffman).

and much of our current understanding regarding heterogeneity of ventilation was derived from these early Xe¹³³ gas studies (West et al., 1962; Anthonisen and Milic-Emili, 1966; Bryan et al., 1966; Kaneko et al., 1966; Milic-Emili et al., 1966). High concentrations of non-radioactive Xe have been used in conjunction with CT (X-ray computed tomography) imaging for high-resolution quantitation of regional pulmonary ventilation (Gur et al., 1979; Marcucci et al., 2001; Tajik et al., 2002) and ventilation/perfusion ratios (Kreck et al., 2001). Most recently, promising techniques for lung imaging using laser polarized Xe and helium for magnetic resonance imaging (MRI) have been described (Albert et al., 1994; Kauczor et al., 1996; Eberle et al., 2001).

Regional lung ventilation using imaging methods involving tracer or radiopaque gases can be measured quantitatively using single-breath (Ball et al., 1962; Tajik et al., 2002) or multi-breath equilibrium techniques (Bunow et al., 1979; Gur et al., 1979, 1981; Murphy et al., 1989; Marcucci et al., 2001). While a single breath technique provides information related to the distribution of the inspired gas under static conditions, multi-breath equilibrium techniques allow for the measurement of the regional distribution of ventilation under steady-state dynamic conditions (Tajik et al., 2002). West and Dollery (1960) evaluated regional pulmonary ventilation by the use of externally placed scintillation counters by measuring the rate of removal of O¹⁵-labeled carbon dioxide after single breath of radioactive gas. Kety (1955) suggested models to measure regional pulmonary ventilation using multi-breath protocols. Most of these models assume that Xe is insoluble in blood and tissue, giving rise to mono-exponential wash-in (WI) and/or wash-out (WO) curves. However, Xe gas is inert and moderately soluble in blood and tissue: the Oswald solubility coefficient of Xe gas is 0.14 at 37 °C for blood and 0.13 for fat (calculated from blood and oil) (Steward et al., 1973). This solubility, under different conditions, may result in uptake of Xe by the blood, storage of dissolved Xe in lung and peripheral tissues, and recirculation of Xe with return to the lung, all of which could affect background levels and/or alveolar accumulation rates. Most of these models, regardless of consideration of Xe solubility in blood and tissue, assume that the Xe wash-in rate is equal to the Xe wash-out rate. Choice between the three different protocols, Xe wash-in (WI)

only, Xe wash-out (WO) only, or Xe wash-in/wash-out (WI/WO) combination, have been based primarily on considerations of convenience or signal:noise ratio (Dollery et al., 1962; Dollery and Gillam, 1963; Brudin et al., 1992; Simon et al., 1998; Kreck et al., 2001) within the assumption of equal WI and WO rates.

Finally, the density and viscosity of Xe gas is 5.44 g/l and 2.25×10^{-5} Pa/s at ambient temperature, respectively (Anonymous, 1987). These values are substantially higher than those of the other typical respiratory gases. Previous studies have demonstrated the effect of physical gas properties on pulmonary mechanics, gas exchange, and ventilation distribution (Jaffrin and Kesic, 1974; Wood et al., 1976a,b; Zhang et al., 1995; Calzia et al., 1999; Baumert et al., 2002). Ventilation distribution is further dependent on several additional factors such as lung mechanical properties (regional structure and compliance), external factors (pleural pressure, heart, chest wall effects), and ventilatory parameters (tidal volume, flow rate).

Our observations using the Xe-CT method suggested that, in different regions and under certain conditions, the lung density may not return fully to baseline after a reasonable wash-out period and, further, that WI and WO time constants may differ considerably. Given the above considerations, we sought to examine the assumption that Xe-CT WI and WO time constants are equal during mechanical ventilation of healthy, supine sheep. In addition, we investigated different factors that might influence this phenomenon, including the effects of tidal volume (which, for the same respiratory frequency, alters flow velocity), anatomic region, scanning modes (end-inspiratory (EI) or end-expiratory (EE) image gating), and inspired Xe concentration (affecting overall density and viscosity of the inspire).

2. Methods

2.1. Animal preparation

This protocol was approved by the University of Iowa Institutional Animal Care and Use Committee. All animal studies were performed within guidelines for animal care defined by the American Physiological Society and the National Institutes of Health.

Fifteen adult sheep (30–40 kg) of either sex were studied. Sheep were pre-medicated with I.M. ketamine

(2 mg/kg) and acepromazine (0.67 ml/kg). The sheep were anesthetized with inhaled isoflurane (1–2%) via nose cone until intravenous access was obtained, after which deep anesthesia was maintained with continuous intravenous infusion of propofol (12 mg/kg/h) titrated to heart rate and reflexes.

After tracheotomy was performed and the trachea intubated with a cuffed endotracheal tube (9.0 mm i.d.), the sheep were mechanically ventilated (10 ml/kg, 12–15 breaths/min) with a Harvard piston pump respirator. Liquid filled pressure catheters were inserted into a carotid artery (blood pressure monitoring) and jugular vein via cutdown procedure. With the guidance of a fluoroscope, catheters were advanced into the right main pulmonary artery (pressure monitoring and administration of anesthesia and fluid) or right ventricle outflow tract (contrast injection).

After instrumentation, sheep were transported to the scanner facility, placed supine on the scanner table, and connected to and ventilated by a Harvard piston pump respirator. The sheep were relaxed with a 1mg intravenous injection of pancuronium bromide. Airway pressure and ECG were monitored using an IBM compatible computer equipped with a standard laboratory A/D converter board and a customized Labview 7.0 (National instruments, Austin, TX)-based PC software. The software was programmed to correlate physiologic information with scanner events by triggering the pulse of the scanner X-ray timed to the ventilation cycle. During a Xe study, Xe was delivered via a specialized delivery device (Enhancer 3000, Diversified Diagnostic products, Houston, TX) into the inhalation side of a Harvard piston ventilator. The Enhancer 3000 allows for control of concentration of Xe and oxygen gas in a closed circuit system, using a CO₂ absorber along with Xenon and oxygen sensors to allow for maintenance of a constant concentration of these gases on the inhalation side of the circuit during a WI maneuver. Throughout the study, deep anesthesia was maintained with continuous I.V. drip (12 mg/kg/h) of propofol titrated to heart rate and reflexes. The sheep were euthanized with sodium pentobarbital (60 mg/kg) and concentrated KCl after completion of the study.

2.2. Imaging protocols

Before each imaging protocol, the lungs were inflated to total lung capacity (30 cmH₂O airway pres-

sure) 3–5 times for the purpose of (1) assuring a constant volume history, (2) promoting maintenance of apnea during scanning and (3) minimization of dependent atelectasis.

2.2.1. Image specifications

All scans were performed in our research dedicated Philips MX 8000 scanner which allowed for the acquisition of four high-resolution (up to 24 line pairs per cm) images per scanner rotation with a gantry rotation speed of 0.5 s per revolution.

With the lungs held at 0, 10, 15 and 30 cmH₂O airway pressures, volumetric images of the lungs were obtained for purposes of being able to evaluate airway geometry and to select locations for Xe-CT studies. This scanner was set at 90 kV and 120 mAs for the multi-breath axial scanning protocol. All images were reconstructed using a 512 × 512 and a “standard” image reconstruction kernel. Slice thickness and increment was set at 4 mm × 2.5 mm and in plane pixel size was 0.449 mm × 0.449 mm, resulting from both image field of view of 22.6 cm.

2.2.2. Xe-CT ventilation protocols

For these multi-breath dynamic imaging series, respiratory gating was used.

Protocol 1. In protocol 1, a series of 130 consecutive EE CT scans were obtained in three animals during Xe-WI (55% Xe–25% oxygen) and WO: seven baseline (28 s), 63 Xe-WI (252 s), and 60 Xe-WO (240 s). In addition, a control image set without Xe delivery was collected for 520 s in one animal. For this study, the ventilator was set to a tidal volume (V_T) of 10 ml/kg. Image location was chosen from the volumetric spiral scan at FRC such that slices were gathered at a location centered half way between the diaphragm dome and the carina. Data from this protocol were used to investigate the characteristics of the Xe signal in the blood and to determine the optimal WI times for subsequent xenon studies.

Protocol 2. Findings from protocol 1, discussed in the results section, demonstrated that the number of time points needed to avoid confounding signals from blood born Xe gas returning from peripheral stores. Thus, in protocol 2 axial scans were gated to 60 consecutive breaths. Six supine sheep were studied in this protocol. Image acquisition was gated to occur at both the EI and EE time points of each breath and

subsequently separated into the inspiratory and expiratory series for separate evaluation of regional Xe-WI and WO characteristics. The 60 breaths were as follows: seven baseline breaths (room air); 33 WI breaths 55% Xe and 25% O₂; and finally 20 WO breaths on room air. The protocol was repeated at tidal volumes of 7 ml/kg, 10 ml/kg, and 13 ml/kg, with respiratory-frequency held at 15 breaths/min, and for slice locations selected at the lung apex and base in each animal. This protocol was performed to investigate the differences in regional Xe-WI and WO rates as a function of tidal volume (velocity), and inspiratory versus expiratory gating modes.

Protocol 3. Protocol 3 consisted of a series of 60 consecutive breaths as in protocol 2, imaging only at EE and repeated with 30, 40, and 55% inspired Xe concentration. This study was carried out in a separate group of six supine sheep. All scans were performed at a tidal volume of 15 ml/kg, a respiratory rate of 10 breaths/min. For these studies we centered our imaging planes only at the basal location (half way between the carina and the diaphragm dome). The purpose of this protocol was to investigate the effect of Xe concentration on the difference of Xe-WI and WO rates. The hypothesis was that, as Xe concentration changed, the differences in WI and WO rates should vary if gas density and viscosity played an important role in these differences.

Protocol 4. As will be shown in the results, dependent, lung regions (but not non-dependent lung regions), failed to return to baseline density in protocol one. Because this paralleled the distribution of blood flow, we wished to test whether WO–WI differences were related to the amount of blood flow to a given lung region. If WO–WI differences were related to the Xe signal in blood returning from the peripheral circulation, we reasoned that these differences should be magnified in regions where the signal was strong enough to affect the WI and/or WO curves. In regions where regional blood flow was low (which also tended to be regions where the per voxel blood volume was also low) then the blood signal would have little to no effect on the WI/WO rates. These studies were performed on the supine position in the same six animals used for protocol 2. Regional pulmonary blood flow was measured through the evaluation of first pass kinetics of a radiopaque contrast bolus (Wolfkiel and Rich, 1992). Following three recruitment maneuvers to

TLC, the lungs were held apneic at 0 cmH₂O airway pressure and images were obtained at 30 time points by triggering scans at the peak of the QRS complex of the ECG signal. After three baseline images were obtained, nonionic radiopaque contrast agent (Iohexol, Amersham, UK) was administered by a bolus injection of 0.75 ml/kg over 2 s via a powered injector (Medrad) connected to a 7F multiple-side-hole catheter placed in the right ventricular outflow tract.

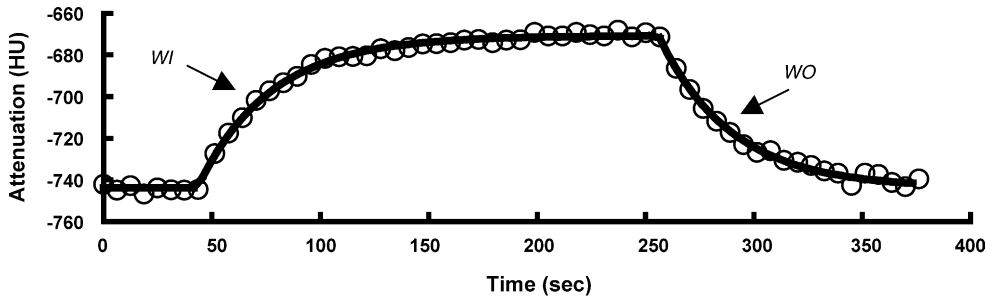
2.3. Ventilation image analysis

The images were transferred to our PC workstations and analyzed using customized software (Time Series Image Analysis or TSIA). For protocol 1, we visually evaluated the time intensity curves in regions of interest placed in the dependent, mid and non-dependent lung regions to gain an initial understanding of the characteristics of the data sets being gathered.

In protocol 2, as a first step, each slice was segmented to separate lung field from the mediastinum, chest wall (rib cage and diaphragm), and myocardium. The area of lung parenchyma was sampled automatically using a regular grid pattern and an ROI size of 2.15–2.79 mm, with 2.5 mm slice thickness. The mean attenuation in each ROI was measured in each image in the series, plotted as a function of time, and ventilation or perfusion parameters were derived using non-linear curve-fitting routines as describe below.

2.3.1. Ventilation

In order to calculate the ROI ventilation time constants, we fitted each regional this WI/WO curve to a single-compartment exponential model using a non-linear least squares curve-fitting procedure which allowed independent time constant assessment for WI and WO curves. One example WI/WO curve is depicted with its associated equation and parameters in Fig. 1. From these curves, specific ventilation (ventilation per unit volume) was calculated as the inverse of the time constant, based upon the model first proposed by Kety (1955). Kety's model of inert gas exchange is applicable to gases with both high and low solubility in blood and tissue, assuming that the inhaled concentration of an inert gas is held constant and alveolar ventilation is treated as a continuous process. For the special case of very low solubility in blood, Kety's model can be



$$D(t) = \begin{cases} t < T_0 : D_0 \\ t_0 \leq t < t1 : D_0 + (D_f - D_0) \left(1 - \exp \left[- \frac{(t - T_0)}{\tau_{wi}} \right] \right) \\ t \geq t1 : D_0 + (D_f - D_0) \cdot \left(1 - \exp \left[- \frac{(t1 - T_0)}{\tau_{wi}} \right] \right) \left(\exp \left[- \frac{(t - t1)}{\tau_{wo}} \right] \right) \end{cases}$$

Fig. 1. Diagram of curve fitting for WI and WO Xe-CT curves. This curve derived from a scanning protocol which used a seven breath baseline, 33 breath WI, and 20 breath WO sequence. Note that the tail of WO curve approximates the initial baseline. The time constants for WI [τ_{wi}] and WO [τ_{wo}] are indicated. The curve equations are given in the lower half of the figure.

described as a simple exponential function.

$$C_A = C_i(1 - \exp(-k \times t))$$

where C_i is the concentration of inspired gas at time t , C_A the concentration (amount) of gas present in the lungs at equilibrium and is related to volume, and k the rate constant that relates alveolar ventilation to alveolar volume (\dot{V}/V_{gas}), called specific ventilation.

To eliminate regions containing major pulmonary blood vessels and airways, data were filtered using two criteria: SSR (summed squared residual) less than 150 (Simon et al., 1998), and air fraction between 40 and 90% (Hoffman et al., 1986). The sagittal slice images were divided into three regions as described in Fig. 2.

Xe-WI and WO rates were compared: (1) apex versus base (2) dependent, middle, non-dependent (3) EI versus EE scans (4) tidal volume at 7, 10, and 13 ml/kg.

In protocol 3, regional perfusion was evaluated.

2.3.2. Perfusion

In order to determine the relationship of perfusion to the difference of WI and WO rates, regional pulmonary blood flow was calculated from contrast injection images using a single compartment model. In this model, flow is proportional to maximal enhancement (Gould, 1992; Tajik et al., 1993). The assumption of

this model is that tissue accumulation of indicator is complete before the indicator washes out significantly.

$$\frac{F_i}{V_{voxel}} = \frac{HU_{t,pk} - HU_{t,base}}{\int_0^\infty (HU_{pa}(t) - HU_{pa,base}) dt}$$

where F_i is the flow to the tissue from main feeding vessel, V_{voxel} the volume of parenchyma present in the

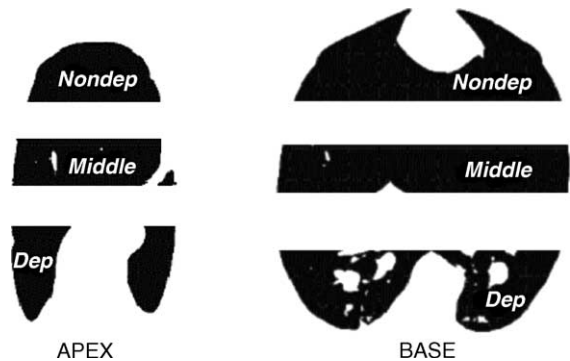


Fig. 2. Visual depiction of the three vertical regions evaluated for each of the four axial slices sampled at the lung apex and base. WI and WO rates were determined for each of these levels which represent the non-dependent 20%, middle 20% and dependent 20% of the lung in each slice.

region of interest, HU_{pa} the Hounsfield unit of contrast agent in the feeding pulmonary artery, $HU_{pa,base}$ the Hounsfield unit measured prior to the arrival of contrast into pulmonary artery, $HU_{t,pk}$ the Hounsfield unit measured at the peak of the parenchymal dilution curve, $HU_{t,base}$ the Hounsfield unit measured prior to the arrival of contrast into the region of interest. The ratio of the peak HU in a ROI placed over lung parenchyma to area of the arterial input curve gives flow per volume of the region (ml/min/ml). Examples and their corresponding plots of input and output data are shown in Fig. 3, where an input ROI is chosen in the center of the feeding pulmonary artery and the output data are selected from the lung parenchyma. A non-linear model of the Marquardt method is fit the gamma variate function to the concentration–time curve. The fitted input and output curves are used to calculate the volume normalized pulmonary blood flow. To remove samples (ROIs) containing major pulmonary blood vessels (veins and arteries) and major airways, two criteria: (1) air fraction between 40 and 90%; (2) blood fraction between 2 and 50% were applied to data.

2.4. Statistical analysis

All data are presented as means \pm S.D. A paired *t*-test was used to compare differences of time constants (e.g. WI versus WO. EI gating versus EE gating, etc.). For all statistical tests, $P < 0.05$ was considered statistically significant.

3. Results

As shown in the upper panel of Fig. 4, data gathered from a study in which no Xe gas was actually delivered remained quite stable with a variation of ± 7 Hounsfield units (HU: water = 0 and air = -1000). However, as seen in the lower panel of Fig. 4, there was a failure to return to baseline during the Xe-WO period in the dependent and, to a lesser degree, in the middle lung regions. There was a return to baseline in the non-dependent lung regions. During the WI phase, Xe passes from alveolar wall into the blood stream, and is transported to peripheral stores (fat), and plays a role as a Xe-source during the Xe-WO portion of our

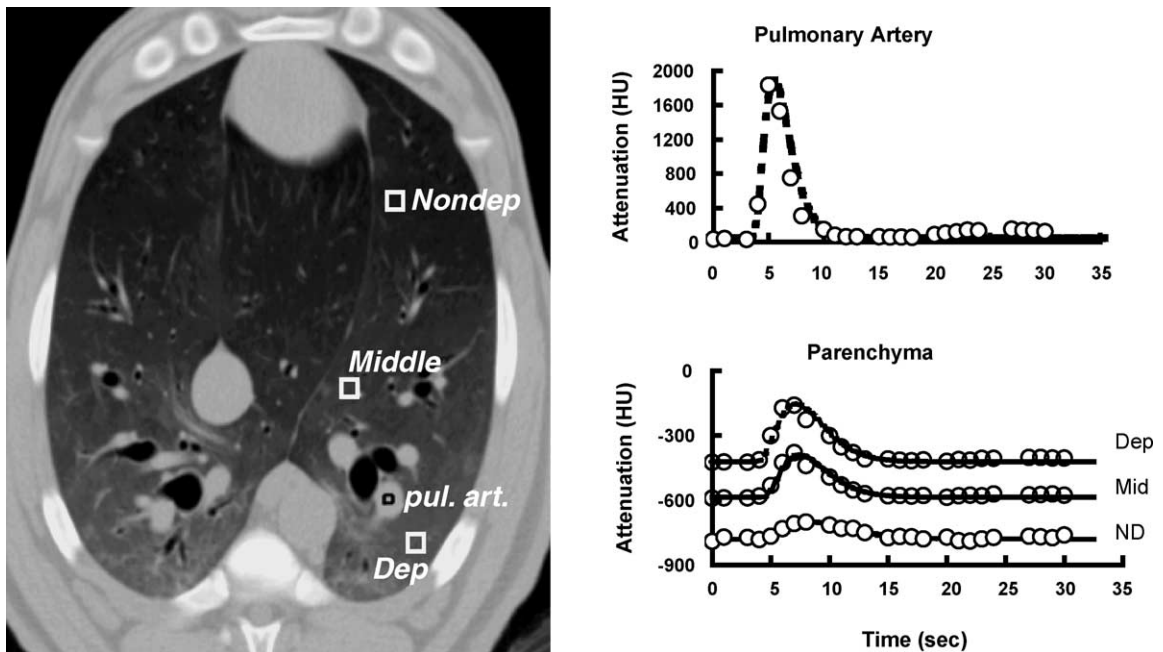


Fig. 3. Time intensity curves derived from scanning the passage of a sharp bolus of contrast material as it traverses the lung field. Arterial curve (right upper panel) and three different parenchymal curves (right lower panel) are demonstrated for regions shown in image. These curves are used to calculate regional pulmonary perfusion parameters.

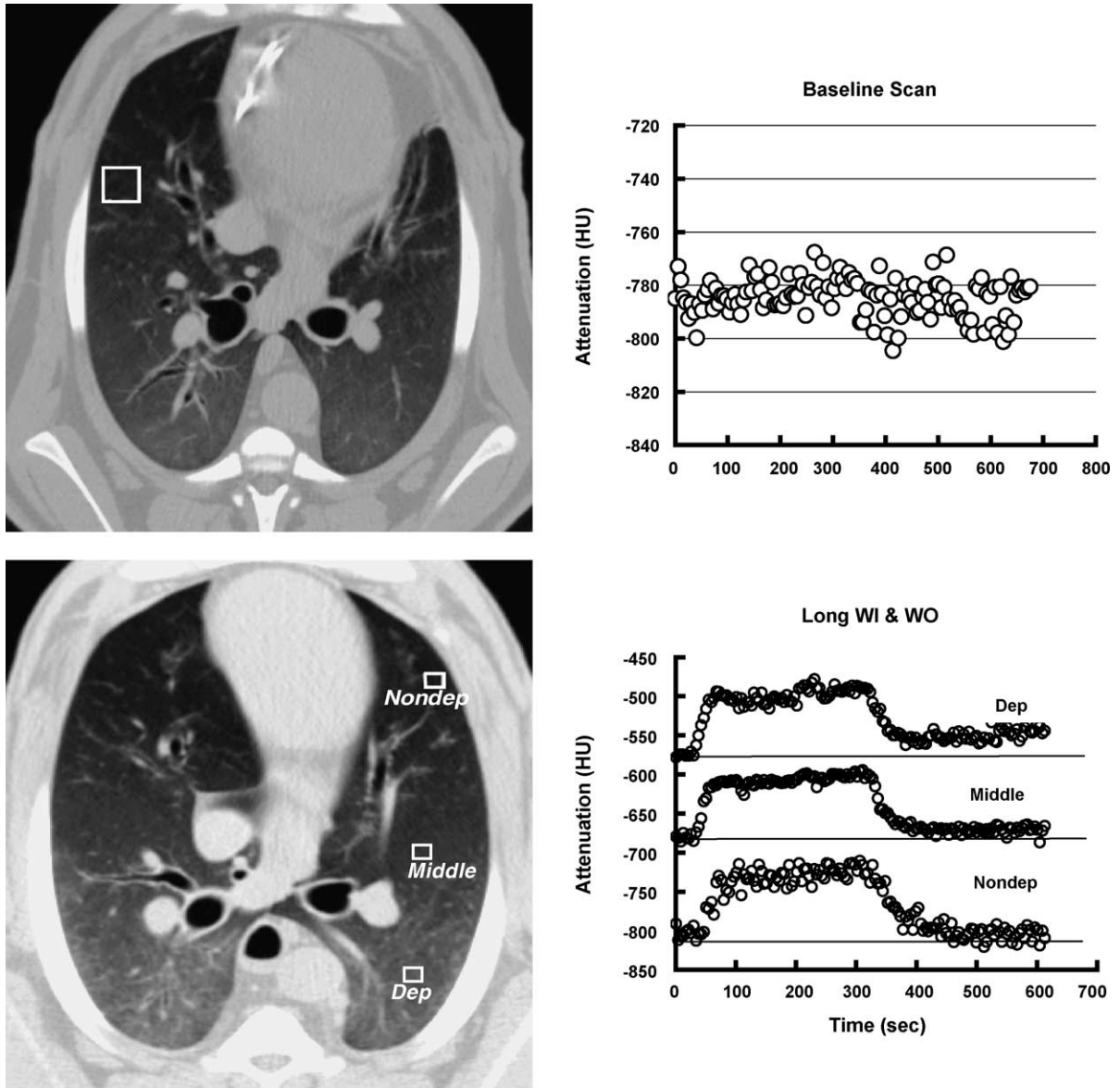


Fig. 4. Upper panel demonstrates the stability of the imaged grey scale values during a simulated Xe protocol. Note that the CT density values remain within ± 7 HU (mean = -784.7 HU) of baseline throughout the scan. Lower left panel shows transverse CT image of a sheep in the supine position along with three ROIs (dependent, middle, non-dependent). Right panel shows regional time attenuation curves corresponding to the three ROIs. The initial baselines are marked at each curve by black horizontal line. From dependent to non-dependent ROIs, the difference of initial baseline and the tail of WO curve decrease, indicating incomplete WO in dependent regions.

imaging protocols. As Bunow et al. (1979) indicated, for radioactive tracers this return of Xe from peripheral stores prevents the tail of the WO curves from returning to baseline, and in this case potentially affects the radiodensity of the lung parenchyma during WI. Therefore,

it is necessary to consider this blood born Xe signal in calculating both WI and WO curves. To minimize the effect of blood born Xe the WI and WO calculations, we limited the number of sample points in subsequent protocols so as to reduce the effect of xenon accumulation

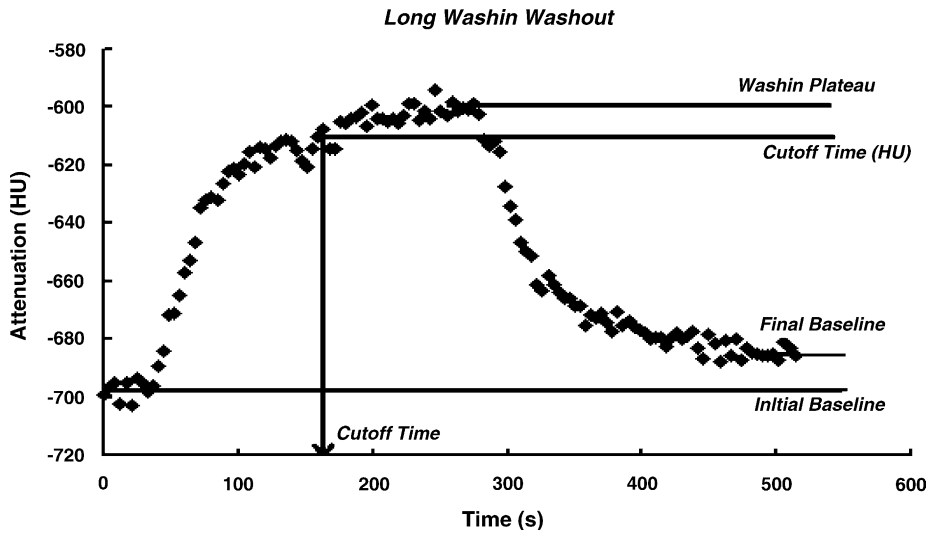


Fig. 5. Position of the optimal cut-off time. Note that the WO curve does not return to baseline, possibly related to the return of xenon gas to the lung from peripheral stores and through simple recirculation. We make the assumption that the peak of the WI plateau should be lowered by the same amount as is reflected in the difference between the initial and final baselines and we identify the time point at which that lower WI plateau occurs. This time point was determined in three sheep and then subsequent protocols in this study switched from the WI to the WO scan phase after this pre-determined number of breaths.

into peripheral stores and its return to the lung. Fig. 5 shows the plot of a WI and WO curve from a representative ROI. To estimate the retention of Xe in blood and tissue after lung WO, an average of seven baseline time points (breaths) was subtracted from an average of the final seven time points (breaths) of WO. Then the magnitude (HU) of the final background activity was subtracted from the average of the last seven time points at the end of the WI curve with the assumption that the plateau is raised by the same amount as the final tail of the WI/WO curve. By finding the point at which the WI curve reaches the predicted plateau (correcting for the shift due to returning Xe stores), we identified the time point at which to stop the WI portion of the study. The average time point was evaluated across all three sheep in protocol 1 and this then determined the timing of subsequent protocols. By reducing the WI time and leaving the WO time the same, in subsequent studies, the WO curves returned to baseline values as shown in Fig. 1. Table 1 shows the mean difference between the final and initial baseline (average: 4.72 [HU]) and optimal cut-off time (average: 33 breath of WI). This cut-off time was used for subsequent protocols.

Fig. 6 summarizes the Xe-WI and WO time constants at the lung apex (left) and lung base (right) for

both dependent and non-dependent regions assessed using EI or EE gating. At both the lung apex and base as well as in the dependent and non-dependent lung regions, the time constants for WI was faster (shorter) than WO. A faster time constant indicates greater regional specific ventilation. As expected from known supine lung physiology (Hoffman and Ritman, 1985), we observed that dependent regions of lung exhibited shorter time constants than did non-dependent lung regions, indicating that the dependent region were better ventilated than non-dependent regions.

Fig. 7 shows histograms representing time constants of WI, WO and WO–WI differences in the apex and

Table 1
Baseline difference and optimal cut-off times

Animal	Supine position, global ROI	
	Final-initial baseline difference (HU)	Optimal cutoff time (br)
1	7.68	31
2	3.79	35
3	2.70	33
Mean	4.72	33
S.D.	2.61	2

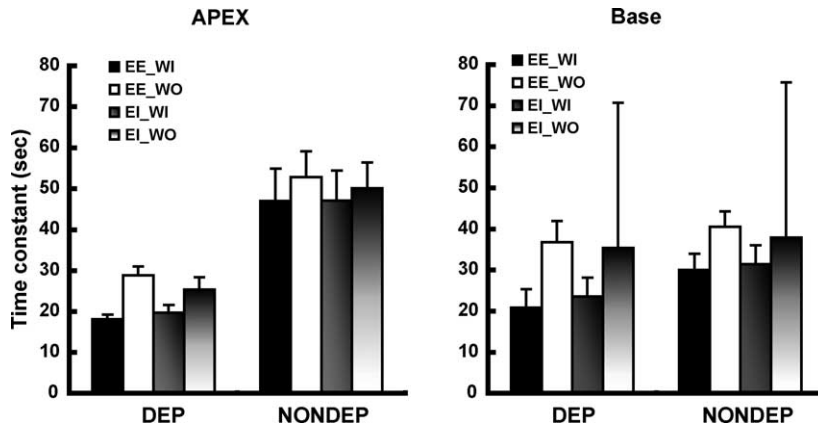


Fig. 6. Note that time constants in the non-dependent regions are longer than in dependent regions, meaning that non-dependent regions are less ventilated than dependent regions. This is in agreement with previous studies. EE, end expiration; EI, end inspiration; WI, wash-in; WO, wash-out.

base of one animal. The histogram of the WO time constants is shifted to the right relative to the WI histogram. Thus, the WO–WI histogram mode is greater than zero. Also, note that the distribution of the WI time

constants is much narrower than that for the WO time constants at both apex and base, indicating that WO time constants are more variable. Despite this, because the mean time constants for WO are greater, the het-

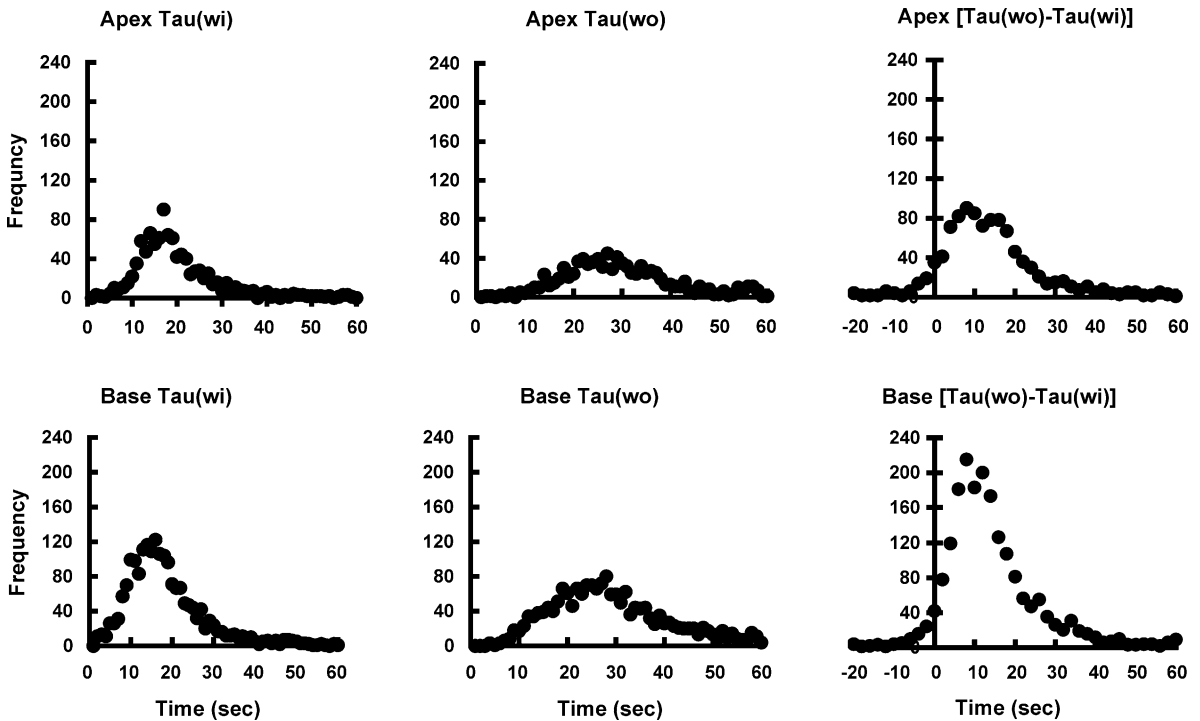


Fig. 7. Histogram of WI, WO, and WO–WI differences at apex and base. Mean WO time constants, and difference of WI and WO time constants were shifted to the right.

Table 2
Coefficient variation (S.D./mean) of WI and WO time constants at apex and base

	APEX		BASE	
	Tau (wi)	Tau (wo)	Tau (wi)	Tau (wo)
1	0.61	0.46	0.68	0.5
2	0.43	0.35	0.58	0.44
3	0.84	0.67	0.68	0.61
4	0.84	0.61	0.71	0.57
5	0.6	0.53	0.8	0.47
6	0.82	0.54	0.75	0.57
Mean	0.69	0.52	0.7	0.52
SD	0.15	0.10	0.06	0.06

erogeneity as measured by the coefficient of variation ($CV = S.D./mean$) of the distributions of WI time constants are significantly larger than the CV's of WO time constants (Table 2, $P < 0.01$).

Example vertical distributions of WI and WO time constant differences are shown in color maps in Fig. 8. Note the color maps of are scaled at the range of -3 to 10 (s) for the lung apex and -3 to 16 (s) for the lung base. The scale difference was necessitated by the fact that the differences are much larger at the lung base compared to the lung apex. Also note that at both the apex and base, the colors indicating the largest differences dominate in the dependent lung region. As shown

in Tables 3 and 4, this finding held for both EI and EE scanning ($P < 0.05$).

In dependent and non-dependent regions, the WO–WI was larger and significantly different at the lung base compared to the apex ($P < 0.05$). This relationship did not hold for the middle sections of the lung.

3.1. Dependence on regional pulmonary blood flow

We postulated that if the WO–WI difference was due to blood flow uptake of tracer gas, the difference

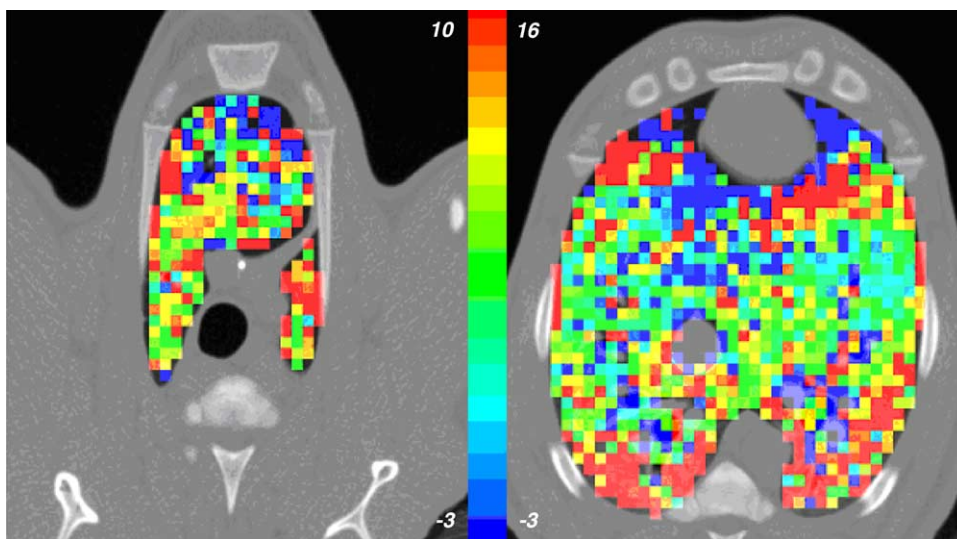


Fig. 8. Color maps of WO–WI time constant differences. Note different scale and that the difference between WO and WI time constant is larger in the dependent region at both apex (left) and base (right).

Table 3
Averaged time constant (WO)–time constant (WI)—end expiration imaging

	EE					
	Apex			Base		
	Nondep	Middle	Dep	Nondep	Middle	Dep
1	-0.28	6.72	8.69	10.13	4.16	12.5
2	2.72	7.16	6.58	9.59	5.65	13.8
3	5.23	4.39	7.02	9.80	5.55	9.86
4	8.71	7.83	27.32	10.8	9.78	26.1
5	12.5	13.33	17.38	12.87	14.95	27.27
6	9.18	15.01	13.72	10.25	10.61	16.19
Mean	6.34	9.07	13.45	10.57	8.45	17.62
SD	4.68	4.14	7.98	1.20	4.08	7.32

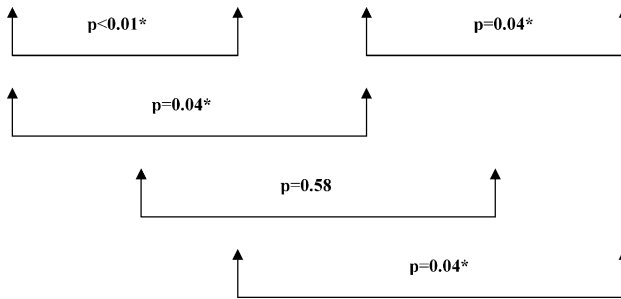


Table 4
Averaged time constant (WO)–time constant (WI)—end inspiration imaging

	EI					
	Apex			Base		
	Nondep	Middle	Dep	Nondep	Middle	Dep
1	1.42	-0.71	1.78	6.22	3.31	6.12
2	-0.51	7.76	5.03	2.1	5.06	12.85
3	0.38	0.28	2.04	2.05	3.08	8.04
4	9.68	8.13	19.36	11.94	6.87	20.53
5	6.53	9.81	10.01	8.48	12.33	20.58
6	8.17	11.98	9.50	13.33	6.79	15.63
Mean	4.27	6.21	7.95	7.35	6.24	13.96
SD	4.37	5.20	6.60	4.79	3.39	6.12

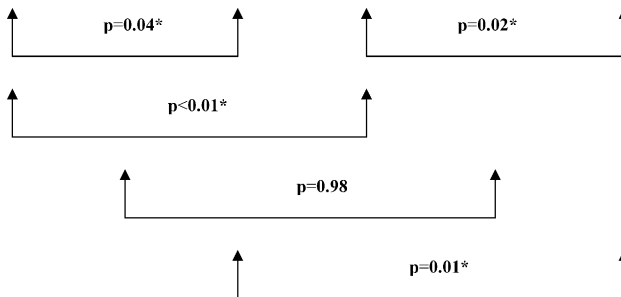


Table 5
Relationship between pulmonary blood flow and averaged time constant (WO)–time constant (WI)

	EE, Base							
	Global		Dependent		Middle		Non-dependent	
	Slope	R^2	Slope	R^2	Slope	R^2	Slope	R^2
1	2.43	0.06	2.40	0.02	3.45	0.08	−3.43	0.01
2	4.00	0.04	2.20	0.01	1.70	0.00	−4.81	0.04
3	6.89	0.06	7.32	0.02	6.74	0.08	3.51	0.01
4	0.08	0.08	0.37	0.13	0.04	0.02	0.01	0.00
5	0.41	0.00	−0.33	0.00	1.37	0.02	−0.73	0.00
6	3.55	0.02	2.45	0.01	4.68	0.04	0.80	0.00
Mean	2.89	0.04	2.40	0.03	2.99	0.04	0.37	0.01
S.D.	2.52	0.03	2.67	0.05	2.45	0.03	3.08	0.01

would be proportional to the local perfusion. Table 5 summarizes the results of a linear regression analysis to test this hypothesis in six sheep under protocol 4. At most, regional pulmonary blood flow could account for only 4% of the difference of the two time constants (mean R^2 value: 0.01–0.04). This lack of correlation between blood flow and WO–WI differences indicate that the signal from Xe returning from peripheral stores is an unlikely explanation for the observed WO–WI time constant differences.

3.2. Dependence on specific ventilation

The relationship between specific ventilation (independent variable) and time constant differences (dependent variable) is shown in Table 6. Based upon a linear regression, R^2 values ranged from 0.03 for the whole lung slice and 0.01–0.11 for three different lung regions. In all cases, the difference in WO–WI time

constants was influenced very little by the regional specific ventilation.

3.3. Effect of EI versus EE scan gating

Comparison of WI and WO time constants in dependent, middle, and non-dependent regions at both the apex and base for EI and EE imaging as well as coefficients of variation of difference of WI and WO time constants for EI and EE imaging of the whole lung slice are shown in Fig. 9. These data indicate that the difference between WO and WI time constant in both the dependent and non-dependent regions at the lung base is significantly larger when measured at EE compared to EI ($P < 0.05$), but not in the middle lung regions.

3.4. Effect of tidal volume

Fig. 10 demonstrates the effect of tidal volume on the differences of WI and WO rates. The left plot shows

Table 6
Relationship between specific ventilation ($s\dot{V}$) and averaged time constant (WO)–time constant (WI)

	EE, Base							
	Global		Dependent		Middle		Non-dependent	
	Slope	R^2	Slope	R^2	Slope	R^2	Slope	R^2
1	0.88	0.04	0.16	0.00	1.41	0.14	1.57	0.01
2	3.57	0.05	5.96	0.09	3.85	0.07	2.56	0.05
3	0.35	0.02	0.42	0.03	0.42	0.03	1.24	0.04
4	0.33	0.01	0.05	0.00	1.01	0.07	5.92	0.24
5	0.51	0.05	0.34	0.03	0.72	0.11	6.49	0.30
6	−0.25	0.01	−0.73	0.04	0.04	0.00	0.33	0.01
Mean	0.90	0.03	1.03	0.03	1.24	0.07	3.01	0.11
S.D.	1.35	0.02	2.44	0.03	1.36	0.05	2.57	0.12

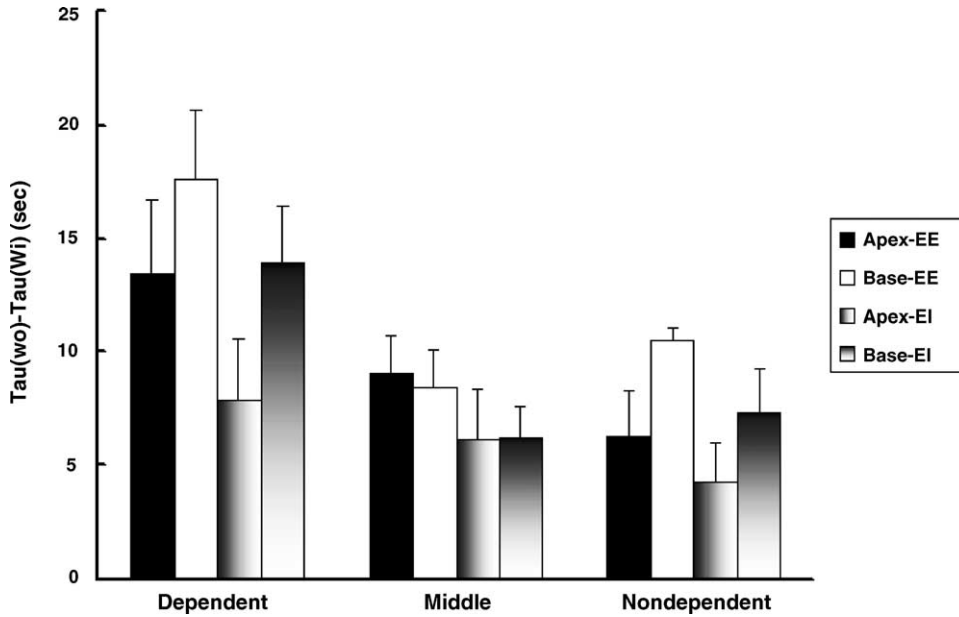


Fig. 9. Effects of EI and EE on WO–WI time constant differences. The WO–WI time constant differences are smaller during EI mode than EE mode in three vertical lung regions at the apex and base.

that, as expected, increasing tidal volume increases ventilation and thus reduces both WI and WO time constants. The right plot shows that as tidal volume increases, however, the difference between regional WI and WO rates decreases. At both the lung apex and base, the WO–WI differences at 13 ml/kg tidal volume were significantly smaller than at 7 ml/kg ($P < 0.05$). However the differences between the individual tidal volume steps did not achieve statistical difference.

3.5. Effect of Xe concentration

The averaged WO–WI time constant differences for the three different Xe concentrations (55, 40, and 30% Xe) in the six supine sheep are shown in Fig. 11. As Xe concentration decreased, the average WO–WI difference decreased: 11.96 ± 4.35 s at 55% Xe, 2.35 ± 3.87 s at 40% Xe, 1.1 ± 3.27 s at 30% Xe (mean \pm S.D.). The average WO–WI difference was

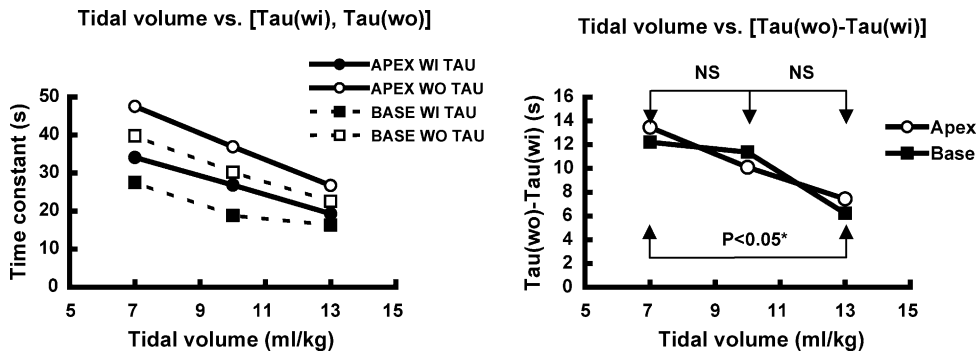


Fig. 10. Effects of tidal volume on WO–WI time constants differences. Each column represents an average of six sheep. Left panel displays time constants at both WI and WO at three tidal volumes at apex and base. Note that as tidal volume decreases, time constants during WO increase more than with WI studies at both the lung apex and base. Right panel shows the difference WO–WI at three tidal volumes at apex and base, indicating that increasing of tidal volume results in decreasing of difference of WI and WO time constant.

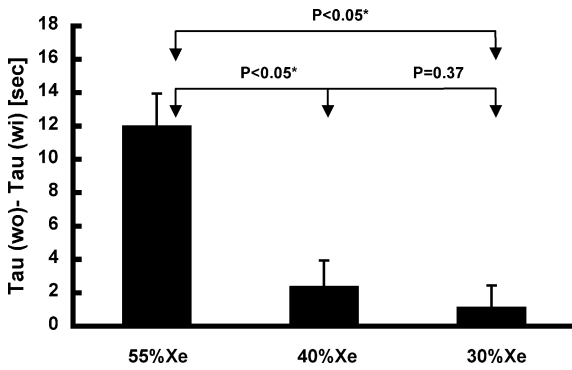


Fig. 11. WO–WI time constant differences derived from data using three different inspired Xe concentrations (55, 40 and 30%). As Xe concentration decreases, the averaged value of WO–WI time constant differences decrease. This WO–WI difference for 55% Xe was significantly greater than that at both 40 and 30% Xe.

Table 7

Density and viscosity of mixed gases

	Density and viscosity of mixed gas		
	55% Xe/air	40% Xe/air	30% Xe/air
Density (kg/m ³)	2.070	1.718	1.543
Viscosity (g/cm s)	0.000183	0.000178	0.000175

significantly greater ($P < 0.05$) at 55% Xe, compared to 40 and 30%. The densities and viscosities of the three gas mixtures are shown in Table 7.

4. Discussion

The aim of this study was to test the hypothesis that the Xe–WI (WI) rate is equal to the Xe–WO rate when using X-ray CT to study regional ventilation. We sought to evaluate the WO and WI time constant relationships as a function of anatomical lung region (apex versus base and dependent versus non-dependent regions), tidal volume (which at fixed respiratory rate and inspiratory time is proportional to flow velocity), and Xe gas concentration (density and viscosity). We further sought to evaluate the influence of gating CT scanning to EE versus EI with the notion that the effect of the conducting airways being filled with alveolar gas versus inspired xenon gas concentrations would possibly serve to reduce the ability to detect differences between the above-mentioned variables. The primary finding of this study is the observation that the Xe–WO rate is dif-

ferent from and slower than the Xe–WI throughout the lung and whether assessed using EI or EE triggering. The WO–WI differences were smaller at the lung apex compared to the base, in the non-dependent compared to dependent regions, and when using EE versus EI gating, large versus smaller tidal volumes, and lower versus higher Xe concentrations. These results suggest that the high density and consequently the lower diffusion coefficient and/or viscosity of Xe gas in combination with anatomic and/or gravitational factors may be responsible for difference seen in the WI and WO rates.

4.1. Minimizing the effect of Xe returning from peripheral stores

We sought to minimize the confounding effects of Xe in returning blood by finding the optimal time point to stop the WI maneuver. Matthews and Dollery (1965) identified three main sources of error in their calculation of regional ventilation from ¹³³Xe, all of which are dependent on the solubility of Xe in blood and tissue. Firstly, they found that their measures were affected by the accumulation of radioactivity in the chest wall and this effect varied with the length of the rebreathing time and individual variations based upon differences in chest wall anatomy at the level of interest. This is a superposition problem with scintigraphy and is not a problem in the case of CT imaging. The second error identified by Matthews was due to the accumulation of ¹³³Xe in the tissue during rebreathing. In the late WI and during the WO phases, depending upon the length of the WI portion of the study, some portion of peripheral Xe gas stores may return to the alveolar space, serving to elevate the WI plateau value and/or inhibit a return to the original baseline after WO (Bunow et al., 1979). The third error arises due to the continuous removal of alveolar Xe by the blood during the rebreathing period. This error could cause an over-estimation of the ventilation in a well-perfused area compared with a poorly perfused area. While some prior studies using Xe scintigraphy tried to correct for these errors by assuming a constant or estimated background signal, others, including prior Xe-CT studies, have not used methods to eliminate these sources of error (although CT by its nature eliminates superposition problems) (Secker-Walker et al., 1975; van der Mark et al., 1980, 1984).

We have sought in this study to minimize the second source of error identified by [Matthews and Dollery \(1965\)](#) using a simple correction which required some assumptions. First, in order to find the optimal WI cut-off time, we assumed that the increased density due to Xe recirculation from the blood in the late WI phase is equal to that observed during the WO phase, based on the reasoning that the volume of distribution and solubility of Xe in the periphery is large relative to the systemic perfusion and thus gas is released at a relatively steady rate during the short period of wash-out. Second, the averaged optimal cut-off time three sheep was obtained by processing the whole lung. This did not take into account possible regional variability. Especially in some less well ventilated non-dependent regions, Xe equilibrium may not be reached at the optimal cut-off time in the WI phase and this could cause greater variability in the measures for this region as has been previously reported by [Simon et al. \(1998\)](#). The optimal cut-off time ($n = 33$ breaths) was obtained at a fixed tidal volume (10 ml/kg) and respiratory rate (15 breaths/min). Because Xe equilibration is dependent on respiratory parameters, the optimal cut-off time could vary based on these values. Finally, if blood carries Xe away from the lung at a faster rate than Xe is returned to the lung from peripheral fat stores (which is likely) then the WI rate in our studies could be underestimated, in which case the WO–WI differences would actually be greater than are estimated by our current measures. Despite these limitations it is our estimate that we have minimized the effect of Xe-return on the WO calculations as evidenced by the results shown in [Table 5](#) which demonstrates that blood flow has essentially no correlation with the observed WO–WI differences.

[Secker-Walker et al. \(1973\)](#) found that the WI rate was 65.2% longer than WO rate (an opposite relationship to ours) before correcting for background activity, but after background correction the difference of Xe-WO and WI rates was reduced to 7.5%. Our results indicated that the WO rate was 39% longer than WI at the base and 27% longer at lung apex. There are several possible reasons for the different results between these studies. First, because of the superposition problems, cross talk amongst detected regions, and the inherent poor spatial resolution of scintigraphy (several centimeters at best) each region of interest may not be fit well by single compartment models. Another expla-

nation may lie in the fact that radioactive studies use only trace amounts of Xe gas compared to our studies which ranged from between 30 and 55% Xe gas concentrations. Our studies demonstrated that the WO–WI differences were increased as a function of gas concentration. In fact, as discussed below, we believe that the WI versus WO effects may very likely be related to the interactions of gas density and viscosity with anatomic and gravitational factors.

Several studies showed that Xe may affect measurement of respiratory mechanics such as airway pressure and pulmonary resistance due to its higher density (ρ) and viscosity (η) ([Table 7](#)) ([Forkert et al., 1975](#); [Drazen et al., 1976](#); [Wood et al., 1976a,b](#)). While most previous studies have agreed that there is an increase in airway pressure during Xe inhalation, the effect of Xe inhalation on pulmonary resistance is controversial. [Zhang et al. \(1995\)](#) showed that pulmonary resistance was increased by use of 70%, but not 50% Xe. However, after correction for pressure signal artifacts by [Calzia et al. \(1999\)](#) as well as for gas density and viscosity under simplified assumptions of flow patterns by [Baumert et al. \(2002\)](#), there were no significant differences in pulmonary airway resistance using 70% Xe. Based on these findings, it is unlikely that pulmonary resistance due to higher density and viscosity of Xe gas causes the difference of WI and WO flow rates obtained using 55% Xe gas in this study.

As shown in [Table 2](#), we have found that WI time constants are more heterogeneous than WO. [Paiva and Egel \(1979\)](#) proposed a mechanism based on the interaction between diffusion and convection in a heterogeneous lung, implying that inspired and alveolar gas during inspiration are mixed by interaction of convection and diffusion in a uniform lung. While convection dominates in the large airway and diffusion dominates in the peripheral lung, in the intermediate size airway interaction of convection and diffusion can cause sharp diffusion fronts that can play a dominant role in distribution of gases in the lung. Based upon the work of [Paiva and Egel \(1979\)](#), if the inspiration of heavier gas (Xe) causes the formation of a diffusion front distal to the bifurcations during Xe-WI (heavy gas WI into a light gas), but during Xe-WO, the diffusion front is formed mouthward of the bifurcation due to the inspiration of lighter air into a resident denser gas, there would be greater heterogeneity of regional time constants during WI than WO, consistent with our findings.

As shown in Fig. 11, as Xe concentration decreased from 55 to 40 and 30%, the WO–WI difference in time constants was significantly decreased, which may be explained by Rayleigh–Taylor instability. This phenomena describes the hydrodynamic effect that occurs when a heavy fluid is accelerated into a light one. In 1980, Lord Rayleigh first discovered this notion for fluid in a gravitation field and in 1950 (Rayleigh, 1883), Sir Geoffrey Taylor (Taylor, 1950) extended it by applying this to all accelerated fluids. It is not necessary for Rayleigh–Taylor instabilities to take place in a gravitational field, which means that when a light fluid runs into a slower, heavy fluid, a deceleration that causes the overturn occurs. Based on the notion of Rayleigh–Taylor instability, when the heavy Xe gas encounters lighter air in the airway during Xe wash-in, Xe gas is accelerated, resulting in faster Xe–WI rates, but during Xe wash-out by air, a light gas encounters heavy Xe gas, and the front is very stable, resulting in a more even distribution of the air to both dependent and non-dependent regions, thus resulting in a slower Xe–WO rate, especially in the dependent lung regions.

Our result showed that the difference of Xe–WI and WO rates were larger in the dependent regions and at the lung base than in the middle and non-dependent regions and at the lung apex. These anatomic differences are paralleled by gradients of both pulmonary ventilation and perfusion that in turn could possibly contribute to WO–WI differences. However, WO–WI differences were essentially uncorrelated with regional ventilation ($R^2 = 3\%$) or perfusion ($R^2 = 4\%$), suggesting that these factors are not important.

Using similar Xe–CT methods as used in the current paper, Tajik et al. (2002) demonstrated a redistribution of regional ventilation with increasing inspiratory flow rate while keeping tidal volume constant, suggesting that the pathway geometry (conductance) becomes more important in the distribution of air flow at high flow velocities due to the dominance of inertial term in flow equation. Their result indicated the dorsal, diaphragmatic region of the pig lung (dependent lung region in a supine pig) received increased ventilation at higher flow rates due to favorable airway structure. They suggested that the monopodial branching pattern found in most mammals other than humans provides a major airway path traversing to the dorsal diaphragmatic region of the lung. The low resistance of this major conducting airway to that region in the supine

posture may lead to short dependent lung time constants (Otis et al., 1956). It is our hypothesis that the observed Xe–WI and WO rate differences are likely due to the interaction between the asymmetrical inspiratory/expiratory airway geometry, gravitational forces and the variable density/viscosity of the inhaled versus resident gases (Rayleigh–Taylor instabilities upon wash-in as described above).

Interestingly, during the extended wash-in period the density of the non-dependent regions appeared to slowly and continuously rise while the dependent regions reached a plateau (Fig. 4). One explanation for this effect could be the presence of intraregional heterogeneity, with the presence of a slow compartment within the voxel (Simon and Venegas, 1994; Melo et al., 2005) although this might be unusual in otherwise normal sheep lungs. Alternatively, if there is preferential flow of the Xe tracer to dependent regions, this late non-dependent rise could be due to a redistribution of Xe from the dependent to the less well ventilated non-dependent regions via the common dead space. However, a likely explanation is that the non-dependent regions simply have a much slower over-all time constant.

While some previous studies have chosen to scan their subjects at end inspiration in order to maximize signal (Robinson and Kreel, 1979; Kreck et al., 2001), others have used EE imaging because of the more reliable return to a consistent lung volume (Marcucci et al., 2001), particularly important to reduce noise with CT imaging (Simon et al., 1998). An additional consideration is that the conducting airways are filled with the inspired concentration of Xe gas at EI, whereas at EE the conducting airways are filled with alveolar gas (Tajik et al., 2002). As a result, scanning at EI could cause regional parenchymal density to be influenced by partial-volume effects from the fresh Xe gas from conducting airways in the ROI. The current study findings demonstrate that imaging at EI masks the WO–WI differences and, possible, might similarly eliminate other important differences in lung physiology.

Crawford et al. (1986) reported that, at a constant alveolar ventilation, convection-dependent inhomogeneity among larger units (interregional) determined at more proximal branchpoints increases with increasing tidal volume. In contrast, they showed that the component of ventilation maldistribution decreases due to the interaction of convection and diffusion in

the lung periphery (intra-regional) when tidal volume increases. Paiva et al. (1984) identified the important role of intraregional zones with parallel units presenting a sequential convective flow in producing an alveolar plateau, indicating that a larger inspired volume will cause a decreased slope using a multibranch point model. Emery et al. (2000) tried to remove many factors affecting heterogeneity such as lung mechanical properties (regional structure and compliance), external factors (pleural pressure, cardiac motion, chest wall), and ventilatory parameters (tidal volume, flow rate) by performing experiments in excised and unperfused lungs. Their findings demonstrated that increasing tidal volume removed the dominant intra-regional component of ventilation heterogeneity, but anatomic dead space and interregional heterogeneity was not influenced. Our findings in this study, whereby differences Xe-WI and WO rates decreased with increasing tidal volume at both the lung apex and base, may be explained by the notion of a dilution effect in which increasing tidal volume causes more uniform mixing of tidal (Xe during WI and air during WO) and resident gas (air during WI and Xe during WO), resulting in decreasing difference of Xe-WI and WO rates.

In summary, we have demonstrated that there are significant differences in Xe-WI and WO rates which depend on Xe concentration, tidal volume, and anatomic location but are not well correlated with regional ventilation or perfusion. These differences seem likely to result from interactions between inhaled and resident gas density and viscosity, airway geometry, and gravity. Our study further suggests that scanning at EE may be important if one wishes to have sensitivity to detailed physiologic information available through Xe-CT imaging. Through the use of the detailed anatomic information available in CT images, coupled with advanced modeling such as computational fluid dynamics, it should be possible to gain important new insights into the phenomena outlined in this paper. Further, with the rapid emergence of new techniques utilizing high concentrations of gases such as hyperpolarized helium (Altes et al., 2004; Altes and Salerno, 2004; Beek et al., 2004) and the use of Xe to image regional lung function via both CT (Simon et al., 1998; Tajik et al., 2002) and MRI (Albert et al., 1994), it becomes of great importance to understand the role of inhaled and resident gas properties in determining characteristics of regional gas turnover rates and, ulti-

mately, for understanding the ventilation that occurs when breathing ambient gas.

Acknowledgements

We thank Dr. Shaher Samrah, Jared Sieren, RTR (CT), John Spahn, for technical help during the study. This study was supported in part by a NIH Bioengineering Research Partnership: RO1 HL-064368.

References

- Albert, M., Cates, G., Driehuys, B., Happer, W., Saam, B., Springer, C.J., Wishnia, A., 1994. Biological magnetic resonance imaging using laser-polarized ^{129}Xe . *Nature* 370, 199–201.
- Almquist, H., Jonson, B., Palmer, J., Valind, S., Wollmer, P., 1999. Regional VA/Q ratios in man using ^{133}Xe and single photon emission computed tomography (SPECT) corrected for attenuation. *Clin. Physiol.* 19, 475–481.
- Altes, T., Rehm, P., Harrell, F., Salerno, M., Daniel, T., Lange, E.d., 2004. Ventilation imaging of the lung: comparison of hyperpolarized helium-3 MR imaging with Xe-133 scintigraphy. *Acad. Radiol.* 11, 729–734.
- Altes, T., Salerno, M., 2004. Hyperpolarized gas MR imaging of the lung. *J. Thorac. Imaging* 19, 250–258.
- Anonymous, 1987. *Viscous of Gases*. CRC Press, FL.
- Anthonisen, N., Milic-Emili, J., 1966. Distribution of pulmonary perfusion in erect man. *J. Appl. Physiol.* 21, 760–766.
- Ball Jr., W.C., Stewart, P.B., Newsham, L.G., Bates, D.V., 1962. Regional pulmonary function studied with xenon 133. *J. Clin. Invest.* 41, 519–531.
- Baumert, J.H., Reyle-Hahn, M., Hecker, K., Tenbrinck, R., Kuhlen, R., Rossaint, R., 2002. Increased airway resistance during xenon anaesthesia in pigs is attributed to physical properties of the gas. *Br. J. Anaesth.* 88, 540–545.
- Beek, E.v., Wild, J., Kauczor, H., Schreiber, W., Mugler, J.r., Lange, E.d., 2004. Functional MRI of the lung using hyperpolarized 3-helium gas. *J. Magn. Reson. Imaging* 20, 540–554.
- Brudin, L.H., Valind, S., Rhodes, C.G., 1992. Error analysis of combined measurement of regional ventilation and V/Q ratio using positron emission tomography. *Phys. Med. Biol.* 37, 1077–1093.
- Bryan, A., Milic-Emili, J., Pengelly, D., 1966. Effect of gravity on the distribution of pulmonary ventilation. *J. Appl. Physiol.* 21, 778–784.
- Bunow, B., Line, B.R., Horton, M.R., Weiss, G.H., 1979. Regional ventilatory clearance by xenon scintigraphy: a critical evaluation of two estimation procedures. *J. Nucl. Med.* 20, 703–710.
- Calzia, E., Stahl, W., Handschuh, T., Marx, T., Froba, G., Bader, S., Georgieff, M., Radermacher, P., 1999. Respiratory mechanics during xenon anesthesia in pigs: comparison with nitrous oxide. *Anesthesiology* 91, 1378–1386.

- Crawford, A.B.H., Makowska, M., Engel, L.A., 1986. Effect of tidal volume on ventilation maldistribution. *Respir. Physiol.* 66, 11–25.
- Dollery, C.T., Gillam, P.M.S., 1963. The distribution of blood and gas within the lungs measured by scanning after administration of ^{133}Xe . *Thorax* 18, 316–325.
- Dollery, C.T., Hugh-Jones, P., Matthews, C.M.E., 1962. Use of radioactive xenon for studies of regional lung function: a comparison with oxygen-15. *Br. Med.* 18, 316–325.
- Drazen, J., Loring, S., Ingram, R., 1976. Effects of gas density, viscosity, flow rate. *J. Appl. Physiol.* 41, 388–395.
- Eberle, B., Markstaller, K., Schreiber, W.G., Kauczor, H.U., 2001. Hyperpolarised gases in magnetic resonance: a new tool for functional imaging of the lung. *Swiss Med. Wkly* 131, 503–509.
- Emery, M.J., Hildebrandt, J., Hlastala, M.P., 2000. Ventilation heterogeneity in excised lobes: effect of tidal volume. *J. Appl. Physiol.* 88, 1659–1671.
- Forkert, L., Wood, L., Charniak, R., 1975. Effect of gas density on dynamic pulmonary compliance. *J. Appl. Physiol.* 39, 906–910.
- Gould, R.G., 1992. Perfusion quantitation by ultrafast computed tomography. *Invest. Radiol.* 27, S18–S21.
- Gur, D., Drayer, B.P., Borovetz, H.S., Griffith, B.P., Hardesty, R.L., Wolfson, S.K., 1979. Dynamic computed tomography of the lung: regional ventilation measurements. *J. Comput. Assist. Tomogr.* 3, 749–753.
- Gur, D., Shabason, L., Borovetz, H.S., Herbert, D.L., Reece, G.J., Kennedy, W.H., Serago, C., 1981. Regional pulmonary ventilation measurements by Xenon-enhanced computed tomography: an update. *J. Comput. Assist. Tomogr.* 5, 678–683.
- Hoffman, E.A., Acharya, R.S., Wollins, J.A., 1986. Computer aided analysis of regional lung air content using three-dimensional computed tomographic images and multinomial models. *Int. J. Math. Model.* 7, 1099–1116.
- Hoffman, E.A., Ritman, E.L., 1985. Effect of body orientation on regional lung expansion in dog and sloth. *J. Appl. Physiol.* 59, 481–491.
- Jaffrin, M.Y., Kesic, P., 1974. Airway resistance: a fluid mechanical approach. *J. Appl. Physiol.* 36, 354–361.
- Kaneko, K., Milic-Emili, J., Dolovich, M., Dawson, A., Bates, D., 1966. Regional distribution of ventilation and perfusion as a function of body position. *J. Appl. Physiol.* 21, 767–777.
- Kauczor, H., Hofmann, D., Kreitner, K., Nilgens, H., Surkau, R., Heil, W., Potthast, A., Knopp, M.V., Otten, E.W., Thelen, M., 1996. Normal and abnormal pulmonary ventilation: visualization at hyperpolarized He-3 imaging. *Radiology* 201, 564–568.
- Kety, S.S., 1955. The theory and applications of the exchange of inert gas at the lungs and tissues. *Pharmacol. Rev.* 3, 1–42.
- Knipping, H., Bolt, W., Venrath, H., et al., 1955. Eine neue Methode zur Prufung der Herz-und Lungenfunktion. *Dtsch Med Wschr* 80, 1146–1147.
- Kreck, T.C., Krueger, M.A., Altemeier, W.A., Sinclair, S.E., Robertson, H.T., Shade, E.D., Hildebrandt, J., Lamm, W.J., Frazer, D.A., Polissar, N.L., Hlastala, M.P., 2001. Determination of regional ventilation and perfusion in the lung using xenon and computed tomography. *J. Appl. Physiol.* 91, 1741–1749.
- Marcucci, C., Nyhan, D., Simon, B.A., 2001. Distribution of pulmonary ventilation using Xe-enhanced computed tomography in prone and supine dogs. *J. Appl. Physiol.* 90, 421–430.
- Matthews, C.M., Dollery, C.T., 1965. Interpretation of ^{133}Xe lung wash-in and wash-out curves using an analogue computer. *Clin. Sci.* 28, 573–590.
- Melo, M., Harris, R., Layfield, J., Venegas, J., 2005. Topographic basis of bimodal ventilation-perfusion distributions during bronchoconstriction in sheep. *Am. J. Respir. Crit. Care. Med.* 171, 714–721.
- Milic-Emili, J., Henderson, J.A.M., Dolovich, M.B., Trop, D., Kaneko, K., 1966. Regional distribution of inspired gas in the lung. *J. Appl. Physiol.* 21, 749–759.
- Murphy, D.M., Nicewicz, J.T., Zabbatino, S.M., Moore, R.A., 1989. Local pulmonary ventilation using nonradioactive xenon-enhanced ultrafast computed tomography. *Chest* 96, 799–804.
- Otis, A.B., McKerrow, C.B., Bartlett, R.A., Mead, J., McIlroy, M.B., Selverstone, N.J., Radford, E.P., 1956. Mechanical factors in distribution of pulmonary ventilation. *J. Appl. Physiol.* 8, 423–427.
- Paiva, M., Egel, L.A., 1979. Pulmonary interdependence of gas transport. *J. Appl. Physiol.* 47, 296–305.
- Paiva, M., Muylem, A.v., Ravez, P., Yernault, J., 1984. Inspired volume dependence of the slope of the alveolar plateau. *Respir. Physiol.* 56, 309–325.
- Rayleigh, L., 1883. *Proc. Lond. Math. Soc.* 14, 170.
- Robinson, P.J., Kreel, L., 1979. Pulmonary tissue attenuation with computed tomography: comparison of inspiration and expiration scans. *J. Comput. Assist. Tomogr.* 3, 740–748.
- Secker-Walker, R.H., Alderson, P.O., Hill, R.L., Markham, J., Baker, J., Potchen, E.J., 1975. The measurement of regional ventilation during tidal breathing: a comparison of two methods in healthy subjects, and patients with chronic obstructive lung disease. *Br. J. Radiol.* 48, 181–189.
- Secker-Walker, R.H., Hill, R.I., Markham, J., Baker, J., Wilhelm, J., Alderson, P.O., Potchen, E.J., 1973. The measurement of regional ventilation in man: a new method of quantitation. *J. Nucl. Med.* 14, 725–732.
- Simon, B.A., Venegas, J.G., 1994. Analyzing ^{133}Xe lung washout curves in the presence of intraregional nonuniformities. *J. Appl. Physiol.* 76, 956–964.
- Simon, B.A., Marcucci, C., Fung, M., Lele, S.R., 1998. Parameter estimation and confidence intervals for Xe-CT ventilation studies: a Monte Carlo approach. *J. Appl. Physiol.* 84, 709–716.
- Steward, A., Allott, P.R., Cowles, A.L., Mapleson, W.W., 1973. Solubility coefficients for inhaled anaesthetics for water, oil and biological media. *Br. J. Anaesth.* 45, 282–293.
- Suga, K., Nishigauchi, K., Kume, N., 1996. Dynamic pulmonary SPECT of xenon-133 gas wash-out. *J. Nucl. Med.* 37, 807–814.
- Tajik, J.K., Chon, D., Won, C., Tran, B.Q., Hoffman, E.A., 2002. Subsecond multisection CT of regional pulmonary ventilation. *Acad. Radiol.* 9, 130–146.
- Tajik, J.K., Kugelmass, S.D., Hoffman, E.A., 1905. An automated method for relating regional pulmonary structure and function: integration of dynamic multislice CT and thin-slice high-resolution CT. In: *Proceedings of the SPIE Medical Imaging 1993*, pp. 339–350.
- Taylor, G., 1950. *Proc. Roy. Soc. A.*, 201.

- van der Mark, T.W., Peset, R., Beekhuis, H., Rookmaker, A.E.C., Woldring, M.G., 1980. An improved method for the analysis of xenon-133 wash-in and wash-out curves. *J. Nucl. Med.* 21, 1029–1034.
- van der Mark, T.W., Rookmaker, A.E., Kiers, A., Peset, R., Vaalburg, W., Paans, A.M., Woldring, M.G., 1984. Nitrogen-13 and xenon-133 ventilation studies. *J. Nucl. Med.* 25, 1175–1182.
- West, J.B., Dollery, C.T., 1960. Distribution of blood flow and ventilation-perfusion ratio in the lung, measured with radioactive carbon dioxide. *J. Appl. Physiol.* 15, 405.
- West, J., Holland, R., Dollery, C., Matthews, C., 1962. Interpretation of radioactive gas clearance rates in the lung. *J. Appl. Physiol.* 17, 14–20.
- Wolfkiel, C.J., Rich, S., 1992. Analysis of regional pulmonary enhancement in dogs by ultrafast computed tomography. *Invest. Radiol.* 27, 211–216.
- Wood, L., Bryan, A.C., Bau, S.K., Weng, T.R., Levison, H., 1976a. Effect of increased gas density on pulmonary gas exchange in man. *J. Appl. Physiol.* 41, 206–210.
- Wood, L., Engel, L., Griffin, P., Despas, P., Macklem, P., 1976b. Effect of gas physical properties and flow on lower pulmonary resistance. *J. Appl. Physiol.* 41, 234–244.
- Zhang, P., Ohara, A., Mashimo, T., Imanaka, H., Uchiyama, A., Yoshiya, I., 1995. Pulmonary resistance in dogs: a comparison of xenon with nitrous oxide. *Can. J. Anaesth.* 42, 547–553.